Experimental study of the kinematic interaction between a cohesive soil and a group of rigid inclusions through dynamic centrifuge tests

Charbel Nohra, Cristian Soriano-camelo, Sandra Escoffier, Zheng Li, Luc Thorel

▶ **To cite this version:**

Charbel Nohra, Cristian Soriano-camelo, Sandra Escoffier, Zheng Li, Luc Thorel. Experimental study of the kinematic interaction between a cohesive soil and a group of rigid inclusions through dynamic centrifuge tests. 8th International Conference of Earthquake and Geotechnical Engineering, Motoki Kazama; Junichi Koseki; Mitsu Okamura; Ryosuke Uzuoka; Ikuo Towhata, May 2024, Osaka, Japan. pp.936-941, 10.3208/jgssp.v10.OS-14-05 . hal-04601090

HAL Id: hal-04601090
https://hal.science/hal-04601090

Submitted on 4 Jun 2024

HAL is a multi-disciplinary open access archive for the deposit and dissemination of scientific research documents, whether they are published or not. The documents may come from teaching and research institutions in France or abroad, or from public or private research centers.

L'archive ouverte pluridisciplinaire **HAL**, est destinée au dépôt et à la diffusion de documents scientifiques de niveau recherche, publiés ou non, émanant des établissements d'enseignement et de recherche français ou étrangers, des laboratoires publics ou privés.

Experimental study of the kinematic interaction between a cohesive soil and a group of rigid inclusions through dynamic centrifuge tests

C. Nohra [i)], C. Soriano-Camelo [ii)], S. Escoffier [iii)], Z. Li [iii)] and L. Thorel [iv)]

i) Ph.D Student, Centrifuges for Geotechnics Lab., Univ Gustave Eiffel, GERS-CG, F-44344 Bouguenais, France.
ii) Post-doctoral Researcher, Centrifuges for Geotechnics Lab., Univ Gustave Eiffel, GERS-CG, F-44344 Bouguenais, France.
iii) Researcher, Centrifuges for Geotechnics Lab., Univ Gustave Eiffel, GERS-CG, F-44344 Bouguenais, France.
iv) Research Director, Centrifuges for Geotechnics Lab., Univ Gustave Eiffel, GERS-CG, F-44344 Bouguenais, France.

ABSTRACT

This paper presents the kinematic interaction that exists between an over-consolidated cohesive soft soil and a group of rigid inclusions by performing two centrifuge tests using the dynamic centrifuge at Gustave Eiffel University in Bouguenais – France. Dynamic centrifuge tests were conducted at a macro-gravity of 50g and were subjected to the same predetermined sequence of seismic events constituted of sinusoidal motions and multi-frequency earthquakes of different peak ground accelerations. Kinematic interaction was studied by analyzing the soil's response in terms of acceleration and displacement at separate locations throughout the soil profile. Boundary effects were verified, and a frequency analysis was conducted in order to study the variation of the soil's predominant frequency. Results indicate that signal transmissions were observed through the inclusions, leading to a larger response at the inclusions' head compared the free field where attenuation was observed during the same ground motion.

Keywords: centrifuge modeling, dynamic, rigid inclusions, kinematic interaction

1 INTRODUCTION

Rigid inclusions (RI's) are long vertical slender elements used to transfer loads throughout compressible soils to underlying competent layers, similarly to classical piles. They differ from piles by the presence of a Load Transfer Platform (LTP) that separates the RI's head from the foundation. RI's are primarily used as reinforcements but contribute to the whole behaviour of the composite foundation system. They are installed as a grid pattern into the weak soil and are used to increase the bearing capacity and reduce foundation vertical settlement. RI's are used typically as an economic substitute for piles either in the case of thick soft layers making the use of piles unsuitable, or in cases where the execution of the rigid connection between the head of the piles and the shallow foundation is difficult. An example for the use of RI's is the Rion-Antirion bridge in Greece (Pecker, 2004)

The performance of RI's and the effect of the LTP have been studied in recent decades under static monotonic loads. A set of recommendations for the conception and design of a RI's reinforcement system under static load was proposed after the French national project ASIRI (ASIRI National Project, 2012). The project ASIRI+ launched in 2019 and aims to develop design procedures for RI's under complex loads (i.e. dynamic, vibration). In the last decade, some studies regarding soil-inclusion-structure interaction of RI's under dynamic load were published. Ha *et al*., (2019) conducted dynamic centrifuge tests to investigate the seismic performance of unconnected pile foundations; Mánica-Malcom *et al*., (2016) used numerical simulations to study the seismic behavior of RI's in soft clay soils. Regarding kinematic interaction, Medina *et al*., (2023) studied the role of rotational kinematic interaction on the seismic response of large offshore wind turbines on monopiles.

This paper aims to discuss the kinematic interaction that exists between a soft soil and a group of RI's by comparing two dynamic centrifuge tests conducted at the Gustave Eiffel geotechnical beam centrifuge in France. Unless specified otherwise, results are presented in prototype scale.

2 MODEL PERPARATION

For both tests, a soil profile consisting of a base layer of 80 mm (model scale) of dense saturated sand, considered here as a stiff layer; followed by 180 mm of consolidated clay-sand mix, considered as the soft layer; and 20 mm of a well graded sand defined as the LTP. Fig. 1 shows a view of the centrifuge models, with the distribution of instruments (described in paragraph 3.2). The free field and reinforced soil tests are mentioned as C-FF and C-RI respectively.

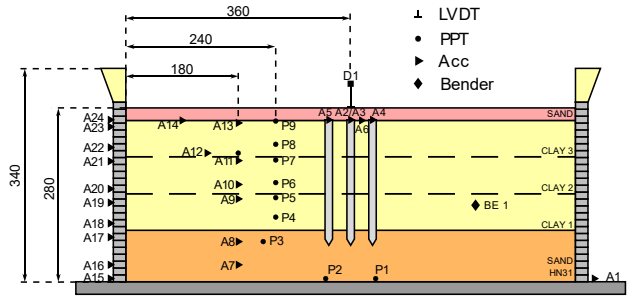

(a) C-RI

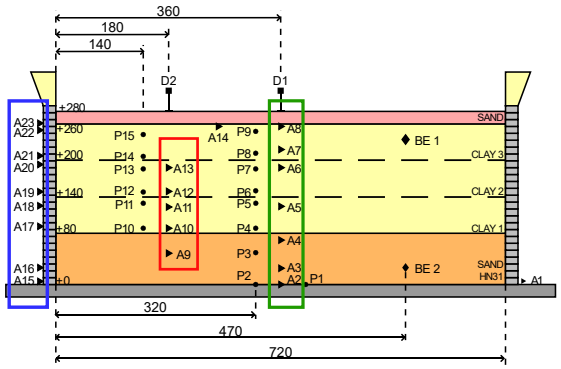

(b) C-FF

Fig. 1. Soil models subjected to centrifuge tests (lengths in mm)

2.1 Container type

For the conducted centrifuge tests, a Laminar Shear Beam (LSB) container was used. It is constituted of superposed frames, each one allowed to slide independently to minimize the friction restricting the soil's movements during shaking events (Esmaeilpour *et al.*, 2023). The container has dimensions of 720×380 mm and a reference height of 340 mm. A rubber membrane was installed inside the LSB to prevent leakage of water and protect it from small soil particles (Soriano-Camelo *et al.*, 2021). LSB containers are therefore used to minimize the boundary effects on the soil that can develop during dynamic load as shown by Lee *et al.*, (2012).

2.2 Base sand layer

The base layer consisted of 80 mm (model scale) of Hostun sand (HN31) and was installed by air pluviation in order to achieve a relative density of 80%. A dense sand is required for the base layer to be modelled as a stiff layer and to prevent liquefaction during shaking. Air pluviation was conducted using a sand pluviator with a slot opening of 4 mm and a falling height of 750 mm. The mechanical properties of the base layer's sand are presented in Table 1 (Benahmed, 2001; Saade *et al.*, 2023). After the pluviation, the sand was saturated by the procedure proposed by Kutter (2013), which involves applying at first a vacuum pressure to remove around 90% of the air in the soil, then flushing the model with CO_2 to replace the air. Note that CO_2 is 50 times more soluble in water than air. After, another application of vacuum pressure and CO_2 flushing is performed in order to remove around 99% of the air before injecting the soil with de-aired water until complete saturation. With this procedure, the degree of saturation can be estimated at around 99.6% (Saade *et al.*, 2023).

Table 1: Mechanical properties of Hostun sand

D_{50} (mm)	e_{min} (-)	e_{max} (-)	G_s (-)	$\rho_{d,\,min}$ (g/cm^3)	$\rho_{d,\,max}$ (g/cm^3)
0.35	0.656	1.049	2.65	1.33	1.66

2.3 Soft clay layer

The soft clay layer is 180 mm (model scale) of thickness (where the RI's were installed), which was divided into three sub-layers of 60 mm each. Each sub-layer was prepared by placing 85 mm of a clay-sand mix slurry prepared with a water content of 60-65%. The slurry is constituted of 80% kaolin clay and 20% Fontainebleau sand. Kaolin clay is best used since it has a relatively higher permeability than other clay making the consolidation time shorter (Pérez-Herreros, 2020). The mechanical properties of kaolin clay are shown in Table 2 (Thorel *et al.*, 2011; Khemakhem, 2012; Escoffier *et al.*, 2022).

Table 2: Properties of Speswhite kaolin clay

γ_s (kN/m^3)	w_p (%)	w_l (%)	I_p (%)	C_c (-)	C_s (-)
26.5	30	55	25	0.269	0.048

γ_s: unit weight of solids w_p: plastic limit
C_c: virgin compressibility w_l: liquid limit
C_s: rebound compressibility I_p : plasticity index

The slurry was then subjected to a pre-consolidation pressure of 120 kPa using a 1g gravity field hydraulic press. During the consolidation, an LVDT (linear variable differential transducer) measured the settlement of the layer. The recorded maximum settlement is approximately 27 mm, meaning that the final thickness of the clay sub-layer is 58 mm, an acceptable value compared to the required thickness of 60 mm. After the consolidation phase of each sub-layer, instruments such as accelerometers, pore pressure transducers as well as bender elements are installed before placing the following layer.

2.4 Load Transfer Platform

For the LTP, sands with angular grains are used in order to assure load transfer to the RIs, therefore a mix of four types of sands having different granulometry are used: HN38, HN34, HN31 and HN06-1. Water is added to the sand mix to achieve a water content of 5%. Assuming that the required unit weight for the sand is 16 kN/m^3, a quantity of sand for 25 mm is first deployed on

top of the clay layer and is compacted using a hammer. The 20 mm thickness is obtained after by trimming 5 mm from the top of the layer. Several measurements of the vertical distance between a reference and the top of the soil are made in order to determine the real thickness of the LTP and its density.

3 INSTRUMENTATION & INPUT MOTIONS

3.1 Installation of RIs

RIs have a length of 200 mm and a diameter of 12 mm. They are constituted of aluminum material with Young's modulus of 74 GPa (Escoffier *et al.*, 2022). A total of seven RI's were used for the kinematic interaction model, four of them being instrumented by four sensors measuring bending moments and two sensors measuring axial forces (strain gauges). The installation was conducted using an apparatus that consists of a transparent guide, in which RIs are placed manually, and a vertical actuator pushed them into the soft layer at a velocity of 0.1 mm/s until the head of the RIs reaches the surface of the soil. Fig. 2 shows the distribution of RIs. The natural frequency of the RI was estimated by hammer impact test at around 3.8 Hz (prototype scale).

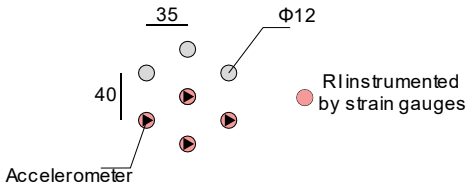

Fig. 2. Plan view of the RI's in the C-RI test (model scale in mm)

3.2 Instrumentation

After the installation of each layer (or sub-layer), sensors such as 1D accelerometers (frequency range: 1 Hz to 20 kHz), noted as "A" and Pore Pressure Transducers, noted as "P" were installed inside the soil (Fig. 1). For the C-FF test, three columns of accelerometers were installed, either at the "center" of the model, either on the LSB container frames that will be called "laminar" or at half distance between both that will be called "quarter". In addition, pairs of bender elements to determine the shear wave velocity were installed in the stiff and soft layers. Finally, LVDT are placed on the soil surface to monitor the settlement (D1 and D2).

3.3 Shaking events

After installing the LSB in the centrifuge, an increase of the gravity level from 0 to 50g, followed by approximately two hours of consolidation. A sequence of twenty ground motions was applied to the model by means of an earthquake simulator (Chazelas *et al.*, 2008). Table 3 shows a list of the input motions with the achieved Peak Ground Acceleration (PGA) measured at the base for the two presented tests. Comparable input motion's PGA were applied for both C-FF and C-RI.

The sequence was constituted of two initial small amplitude earthquakes that were used to determine the soil's predominant frequency; three sets of sine motions with different frequency, each set composed of three motions with increasing PGA; finally, two sets earthquakes, each with different PGA.

Table 3. Signal type and PGA of the sequence's input motions

Signal	PGA (g)	
	C-FF	C-RI
landers 0.05g	0.075	0.072
northridge 0.05g	0.080	0.074
sine 1 Hz 0.05g	0.102	0.119
sine 1 Hz 0.15g	0.217	0.261
sine 1 Hz 0.25g	0.360	0.364
landers 0.05g	0.079	0.079
sine 1.8 Hz 0.05g	0.095	0.086
sine 1.8 Hz 0.15g	0.240	0.275
sine 1.8 Hz 0.25g	0.408	0.397
landers 0.05g	0.088	0.075
sine 2.4 Hz 0.05g	0.073	0.141
sine 2.4 Hz 0.15g	0.191	0.292
sine 2.4 Hz 0.25g	0.313	0.412
landers 0.05g	0.086	0.080
landers 0.15g	0.169	0.196
landers 0.30g	0.312	0.328
northridge 0.05g	0.071	0.084
northridge 0.15g	0.208	0.225
northridge 0.30g	0.433	0.464
landers 0.05g	0.078	0.075

4 CENTRIFUGE TESTS RESULTS

The results obtained from the centrifuge tests on the kinematic interaction between the RI's and the surrounding soft layer are discussed in terms of boundary conditions, transfer function, stress-strain curves and influence of the input motion on the kinematic interaction.

4.1 Boundary conditions

The maximum acceleration profiles of the three columns of accelerometers installed during the C-FF test (Fig. 3) shows for the first set of sines (1 Hz) a good resemblance between the center and the quarter columns, especially in the soft layer, reflecting little boundary effects. The container's response was similar to the other columns during the small (0.05g) and medium (0.15g) amplitude sines, but different during the large amplitude (0.25g). It was also observed that the displacement

response of the soil in ahead the container, meaning that the response is governed by the soil rather than by the container, therefore the model's behavior is not influenced greatly by the LSB.

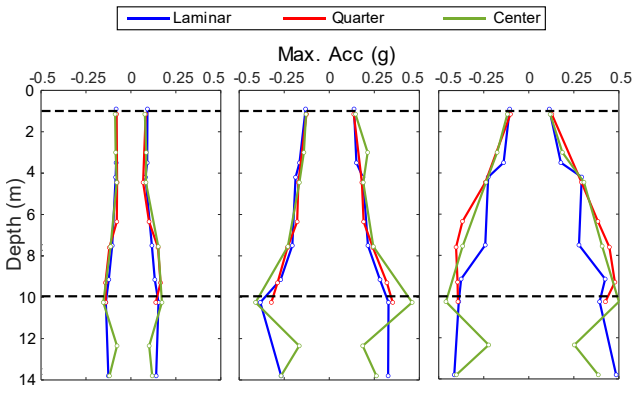

a) Sine 1 Hz 0.05g b) Sine 1 Hz 0.15g c) Sine 1 Hz 0.25g

Fig. 3. Maximum acceleration profile of the three soil columns in the C-FF test.

4.2 Frequency analysis

The predominant frequency of the soil was determined by computing the transfer function (TF) between the soil's base and surface. It corresponds to the ratio of the Fourier transform of the acceleration response at the surface and at the base. Fig. 4 shows the amplitude of two TF computed using the acceleration at the base of the model and the base of the clay layer.

The result shows a similar pattern either using the accelerometer in the sand or in the clay, meaning that the response of the soil's column is mostly controlled by the soft layer (Pérez-Herreros, 2020).

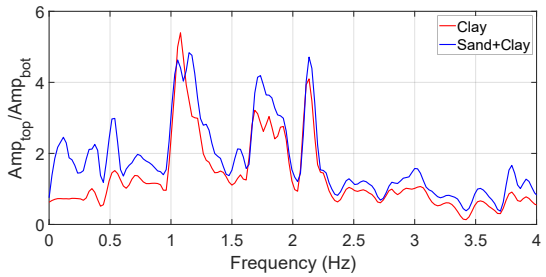

Fig. 4. Transfer function amplitude computed using acceleration response at the model's and clay's base.

A time-frequency analysis using the Stockwell Transform (Moukadem *et al.*, 2015) was conducted to study the evolution of the soil's response during the seismic event. Fig. 5 and Fig. 6 represent the time-frequency representation for the TF between the base (input motion) and the soil's surface (either FF or RI using both tests) during a small and high amplitude earthquake respectively. The results show that prior to the earthquake, frequencies of around 2 – 2.2 Hz are amplified. It corresponds to the frequency of the soil under small distortions (elastic). A drop in the frequency is witnessed during the application of the earthquake: it is small during the small amplitude (1 – 1.1 Hz) and much more pronounced during the large amplitude (0.4 – 0.5 Hz). This means that important nonlinearities and large deformations develop even during the large amplitude, reflecting a degradation of the secant shear modulus and an increase in the damping ratio of the clay. It can be also seen that after the large amplitude motion, the soil recovers part of its properties since the predominant frequency increases, but remains smaller than the small deformation frequency, reflecting permanent damages.

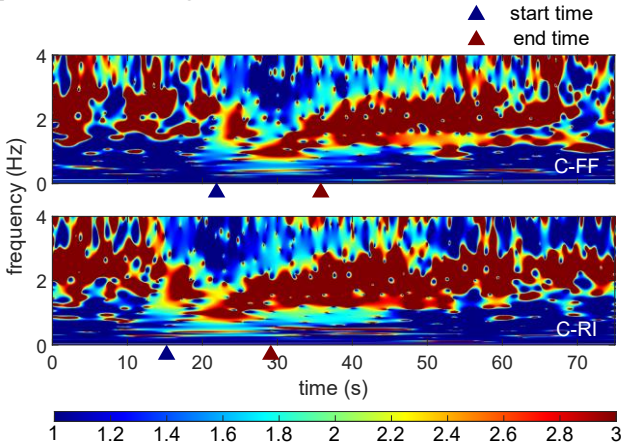

Fig. 5. Time-Frequency representation of the transfer function during a small amplitude (northridge 0.05g).

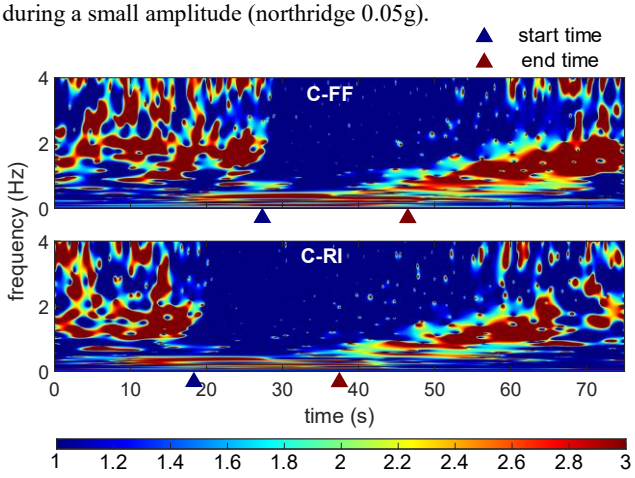

Fig. 6. Time-Frequency representation of the transfer function during a large amplitude (northridge 0.3g).

4.3 Stress-Strain curves

The shear modulus and damping ratio can be quantified by representing the stress-strain hysteresis loops. The time-dependent shear stress and strain were computed using the procedure of Zeghal & Elgamal, (1994): shear stress at the depth z_i was calculated by the equation

$$\tau(z_i,t) = \int_0^{z_i} \rho \ddot{u}(z,t)\, dz \qquad (1)$$

Where ρ corresponds to the density of the soil and $\ddot{u}$ to the acceleration time history recorded by accelerometer i; and shear strain at depth z_i was computed assuming a

1D wave propagation condition and using a first order approximation, expressed as the equation

$$\gamma\,(z_{i-1} < z \leq z_i, t) = \frac{u_{i-1} - u_i}{|z_{i-1} - z_i|} \qquad (2)$$

Where $u_i = u\,(z_i, t)$ is the displacement time history of accelerometer i obtained by double integration of the acceleration. Fig. 7 shows the stress – strain hysteresis loops obtained at three different depths during the two sines 1 Hz 0.05g and 0.15g and for both tests. The secant shear modulus was computed as the average slope of each loop while the damping ratio is calculated by the equation

$$D = \frac{\Delta W}{4\pi W} \qquad (3)$$

Where ΔW is the dissipated energy and W is the elastic energy (Masing *et al.*, 1926). Results show that during both tests and all motions, large shear strain were observed at larger depths, and they decreased with the upward propagation of the signal. High shear strain values reflect important plasticity and irreversibility, as well as energy dissipation, explaining the smaller distortions at shallower depths. Comparing both tests: for sine 0.05g, the distortions and damping ratio during C-FF were larger and the shear modulus is smaller than during C-RI; however, for sine 0.15g, a similar trend was observed only at depths of 6 m and 9 m whereas a small increase in distortions and damping ratio was observed at 3 m. Therefore, it indicates that RI tend to decrease the maximum shear strain and damping ratio overall the soil's column and especially at large depths.

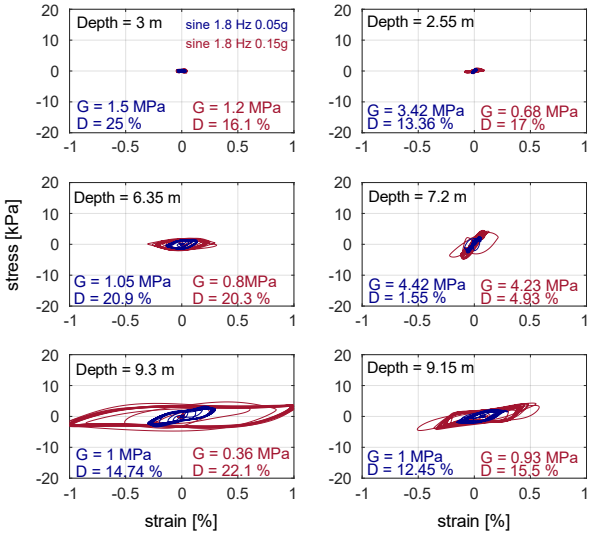

(a) C-FF (b) C-RI

Fig. 7. Stress - strain hysteresis loops calculated during the sine 1.8 Hz 0.05g and 0.15g at three different depths and during both tests

4.4 Influence of the input motion's properties

The effect of the amplitude and the frequency of the input motion on the response of the C-RI was compared with the response of C-FF. Fig. 8 shows the maximum acceleration a_{surf} obtained from accelerometer installed on the cohesive layer surface (either FF or RI's head) with respect to the input motion's PGA.

Regarding the result of C-FF, during sines of 1.8 Hz and 2.4 Hz, a_{surf} is almost the same regardless of the PGA, and is very small compared to the 1:1 line, which means that the input motion's energy dissipated significantly. However, during the Sine 1 Hz input, a_{surf} increases with the PGA until reaching a peak after which it starts to decrease. This might be due to the drop in the predominant frequency when subjected to the large amplitude sine 1 Hz (see paragraph 4.2), making it further away from the frequency of the signal. Therefore, it indicates that as far as the frequency of the base shaking is far from the response frequency of the soil column (1 Hz), the response of the free field is independent of the PGA. However, as observed for the test C-RI, under sine motions with similar PGA, the responses for the three frequencies (1, 1.8 and 2.4 Hz) are relatively similar. Also, at small amplitude motions, the response of the C-FF and C-RI are almost similar, whereas at higher amplitudes, the results of C-RI show an almost linearly increasing relationship with an average slope still smaller than the 1:1. This indicates that even high amplitude motions experience signal transmission through the RIs. Thus, contrary to the FF, the input's PGA has an influence on the response at the RI's head.

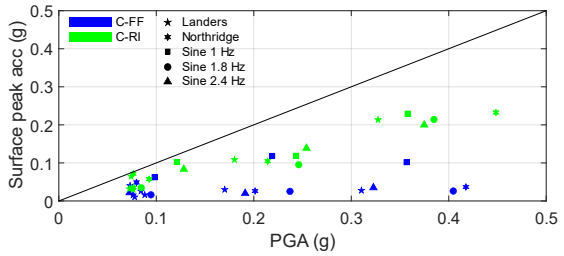

Fig. 8. Evolution of the maximum acceleration and displacement at the surface of the soft layer with respect to the PGA and PGD at the base of the container.

To further investigate, the kinematic interaction factor (KI) – defined as the ratio between the maximum displacements at the head of the RIs and the FF – is represented as a function of the input's frequency in Fig. 9. It is shown that for small PGA, KI < 1 and the results are similar regardless of the frequency (the RI head moves less than the soil). However, for higher PGA, a clear dependence of the frequency is observed. The sine with a frequency of 2.4 Hz witnessed a KI larger than the sine of 1.8 Hz and 1 Hz. Under higher PGA, the displacement response near the RI might be governed by the dynamic properties of the RI and the frequency of 2.4 Hz is closer to the natural frequency of the RI, thus inducing larger displacements at the head. Therefore, the response of the system with RI is not only dependent on

the PGA, but on the combination of the system's (RI+near soil) frequency and PGA of the ground motion.

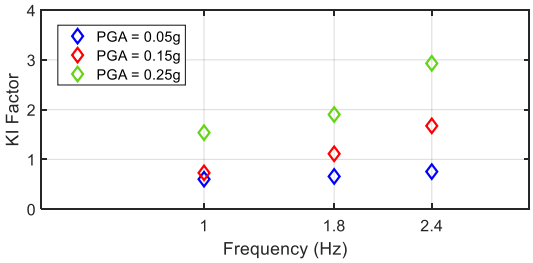

Fig. 9. Kinematic interaction factor as a function of the input's frequency using sine motions.

5 CONCLUSION

The kinematic interaction between soft soil and a group of RI has been studied on two dynamic centrifuge tests. It was observed that boundary effects of the container on the soil's response were little in the region between the RI and the container that can be considered as a free field. The frequency analysis showed that the behavior of the model is very non-linear since the predominant frequency drops even during small amplitude motions. This drop is accompanied by the degradation of the secant shear modulus and an increase in the damping ratio. The RI are seen to decrease the distortions and the damping ratio except at shallow depths. Finally, it was observed that the response at the RI's head is related to the combination of the input motion's PGA and frequency.

ACKNOWLEDGEMENTS

The authors want to thank the French National Research Agency for funding the ASIRIplus_SDS project (ANR-19-C22-0015), as well as the Pays de la Loire region and the Gustave Eiffel University for the Ph.D grant. Special thanks to the GERS-CG technical team as well.

REFERENCES

1) ASIRI National Project (2012). Recommendations for the Design, Construction and Control of Rigid Inclusion Ground Improvements. Retrieved from Presses des Ponts, Paris (FRANCE).
2) Benahmed, N. (2001). *Comportement mécanique d'un sable sous cisaillement monotone et cyclique: application aux phénomènes de liquéfaction et mobilité cyclique.* Doctoral dissertation, Marne-la-vallée, ENPC.
3) Chazelas, J. L., Escoffier, S., Garnier, J., Thorel, L., & Rault, G. (2008). Original technologies for proven performances for the new LCPC earthquake simulator. *Bulletin of earthquake engineering*, *6*, 723-728. DOI: 10.1007/s10518-008-9096-z
4) Escoffier, S., Li, Z., and Soriano, C. (2022). Data Report no. 2 ASIRI+ Project amélioration des sols par inclusions rigides: sollicitations dynamiques et sismiques. Technical report, Université Gustave Eiffel.
5) Esmaeilpour, P., Mamazizi, A., & Madabhushi, G. S. (2023). An overview of the model container types in physical modeling of geotechnical problems. *Soil Dynamics and Earthquake Engineering*, *168*, 107827. DOI: 10.1016/j.soildyn.2023.107827.
6) Ha, J. G., Ko, K. W., Jo, S. B., Park, H. J., & Kim, D. S. (2019). Investigation of seismic performances of unconnected pile foundations using dynamic centrifuge tests. *Bulletin of Earthquake Engineering*, *17*, 2433-2458. DOI: 10.1007/s10518-018-00530-y
7) Khemakhem, M. (2012). *Etude expérimentale de la réponse aux charges latérales monotones et cycliques d'un pieu foré dans l'argile*. Doctoral dissertation, Ecole centrale de Nantes.
8) Kutter, B. L. (2013). Effects of capillary number, Bond number, and gas solubility on water saturation of sand specimens. *Canadian Geotechnical Journal*, *50*(2), DOI: 10.1139/cgj-2011-0250.
9) Lee, C. J., Wei, Y. C., & Kuo, Y. C. (2012). Boundary effects of a laminar container in centrifuge shaking table tests. *Soil Dynamics and Earthquake Engineering*, *34*(1), 37-51. DOI: 10.1016/j.soildyn.2011.10.011.
10) Mánica-Malcom, M. Á., Ovando-Shelley, E., & Botero Jaramillo, E. (2016). Numerical study of the seismic behavior of rigid inclusions in soft Mexico City clay. *Journal of Earthquake Engineering*, *20*(3), 447-475. DOI: 10.1080/13632469.2015.1085462.
11) MASING, G. (1926). Eigenspannungen und verfestigung beim messing. In *Proceedings, second international congress of applied mechanics* (pp. 332-335).
12) Medina, C., Álamo, G. M., & Padrón, L. A. (2023). Contribution of the rotational kinematic interaction to the seismic response of monopile-supported offshore wind turbines. *Ocean Engineering*, *280*, 114778. DOI: 10.1016/j.oceaneng.2023.114778
13) Moukadem, A., Bouguila, Z., Abdeslam, D. O., & Dieterlen, A. (2015). A new optimized Stockwell transform applied on synthetic and real non-stationary signals. *Digital Signal Processing*, *46*, 226-238. DOI: 10.1016/j.dsp.2015.07.003.
14) Pecker, A. (2004). Design and construction of the Rion Antirion Bridge. In *Geotechnical engineering for transportation projects* (pp. 216-240). DOI: 10.1061/40744(154)7.
15) Pérez-Herreros, J. (2020). *Dynamic soil-structure interaction of pile foundations: experimental and numerical study.* Doctoral dissertation, École centrale de Nantes.
16) Saade, C., Li, Z., Escoffier, S., & Thorel, L. (2023). Centrifuge and numerical modeling of the behavior of homogeneous embankment on liquefiable soil subjected to dynamic excitation. *Soil Dynamics and Earthquake Engineering*, *172*, 107999. DOI: 10.1016/j.soildyn.2023.107999.
17) Soriano-Camelo, C. Y., de Almeida, M. C. F., Madabhushi, S. G., Stanier, S. A., de Almeida, M. D. S. S., Liu, H., & Borges, R. G. (2021). Seismic Centrifuge Modeling of a Gentle Slope of Layered Clay, Including a Weak Layer. *Geotechnical Testing Journal*, *45*(1). DOI: 10.1520/GTJ20200236.
18) Thorel, L., Ferber, V., Caicedo, B., & Khokhar, I. M. (2011). Physical modelling of wetting-induced collapse in embankment base. *Géotechnique*, *61*(5), 409-420. DOI: 10.1680/geot.10.P.029.
19) Zeghal, M., & Elgamal, A. W. (1994). Analysis of site liquefaction using earthquake records. *Journal of geotechnical engineering*, *120*(6), 996-1017. DOI: 10.1061/(ASCE)0733-9410(1994)120:6(996).